Insights from Fisher's geometric model on the likelihood of speciation under different histories of environmental change

Ryo Yamaguchi[1] and Sarah P. Otto[2]

[1]Department of Biological Sciences, Tokyo Metropolitan University, 1-1 Minami-Osawa, Hachioji, Tokyo, 192-0397, Japan

[2]Department of Zoology & Biodiversity Research Centre, University of British Columbia, Vancouver, British Columbia, Canada, V6T 1Z4

Corresponding author: Ryo Yamaguchi
Email: ryamaguchi@tmu.ac.jp

Abstract

The formation of new species via the accumulation of incompatible genetic changes is thought to result either from ecologically-based divergent natural selection or the order by which mutations happen to arise, leading to different evolutionary trajectories even under similar selection pressures. There is growing evidence in support of both ecological speciation and mutation-order speciation, but how different environmental scenarios affect the rate of species formation remains underexplored. We use a simple model of optimizing selection on multiple traits ("Fisher's geometric model") to determine the conditions that generate genetic incompatibilities in a changing environment. We find that incompatibilities are likely to accumulate in isolated populations adapting to different environments, consistent with ecological speciation. Incompatibilities also arise when isolated populations face a similar novel environment; these cases of mutation-order speciation are particularly likely when the environment changes rapidly and favors the accumulation of large-effect mutations. In addition, we find that homoploid hybrid speciation is likely to occur either when new environments arise in between the parental environments or when parental populations have accumulated large-effect mutations following a period of rapid adaptation. Our results indicate that periods of rapid environmental change are particularly conducive to speciation, especially mutation-order or hybrid speciation.

Keywords

Ecological speciation, mutation-order speciation, homoploid hybrid speciation, Fisher's geometric model.

Introduction

According to the ecological theory of speciation, populations diverge when exposed to different environmental conditions (Schluter 2000). Metaphorically, populations in different environments are thought to evolve phenotypically across different fitness landscapes, diverging over time as they approach different fitness peaks. This theory can be tested using reciprocal transplant experiments in which the performance of phenotypically divergent populations and their hybrid progeny are measured in both parental environments. The results of such studies often indicate that the environment matters, with phenotypic differentiation and the performance of hybrids depending on the environment (Table 5.1 in Schluter 2000).

An alternative theory of speciation – "mutation-order speciation" – proposes that populations diverging under similar selection pressures may ultimately become reproductively isolated because they accumulate different sets of mutations, some of which are incompatible with one another (Mani and Clarke 1990; Schluter 2009; Schluter and Conte 2009; Mendelson et al. 2014). The focus here is on the reduction in fitness caused by combining genes that have independently spread in different populations, so-called "Dobzhansky-Muller" incompatibilities, regardless of the environment in which hybrids are assayed.

Empirical field studies have suggested that both divergent selection and parallel selection are relatively common (Table 5.2 in Schluter 2000), suggesting that both ecological and mutation-order speciation may underlie the formation of new species.

Experimental evolution studies in the lab have also provided evidence for both ecological speciation and mutation-order speciation. In such studies, multiple independent cultures of organisms are allowed to evolve under either different environmental conditions or identical conditions, following which genetic incompatibilities are measured between the replicate populations. Evidence for ecological speciation has been obtained in studies that have adapted lines to different conditions. For example, Dettman et al. (2007) evolved multiple populations of the yeast *Saccharomyces cerevisiae* in either rich media with high salt or in minimal media with low glucose; in most replicates, hybrid diploids performed significantly worse than the strain that had adapted to a particular local environment. Similarly, Dettman et al. (2008) adapted *Neurospora crassa* to either high salinity or low temperature conditions;

when crossed, reproductive success was lower among hybrids formed from strains adapted to different environments than among hybrids from strains adapted to the current environment being tested.

Evidence for mutation-order speciation includes an experimental evolution study by Kvitek and Sherlock (2011) in *S. cerevisiae* involving multiple replicate populations propagated under glucose limitation. Genomic sequencing revealed that mutations in two genes (MTH1 and HXT6/HXT7) arose repeatedly in different lines but were never found together. Subsequent crosses established that adaptive mutations at each of these two genes were deleterious when combined, reducing the fitness of hybrids. Similarly, a recent study of *S. cerevisiae* adapting in the presence of the fungicide nystatin found that even the first-step mutations that arise during adaptation can be incompatible (Ono et al. 2017). When lines that had accumulated different resistance mutations were crossed, the double-mutants performed less well than either single-mutant in many cases ("sign epistasis"). Sign epistasis was also observed in an experiment with the bacterium, *Methylobacterium extorquens*, evolving to tolerate a genetically-engineered change to how formaldehyde is oxidized (Chou et al. 2014); again, adaptive mutations tended to work poorly when combined.

Previous theoretical studies have predicted the fitness of recombinant hybrids under divergent and parallel adaptation following a period of adaptation with *de novo* mutations (Barton 2001; Chevin et al. 2014; Fraïsse et al. 2016). These models have clarified how segregation of different adaptive alleles reduces hybrid fitness ("segregation load") through the accumulation of different mutations in different populations. Using Fisher's geometric model to track fitness variability among hybrids between independently adapting populations, Chevin et al. (2014) found that segregation load (isolated from extrinsic, environment-dependent, fitness effects) is insensitive to whether adaptation occurred to the same or to different environmental optima (e.g., Figure 2 in Chevin et al. 2014). Segregation load was also found to increase with the dimensionality of the phenotype. Fraïsse et al. (2016) further found that Fisher's geometric model can generate many of the empirical patterns of speciation studies, from Haldane's rule to asymmetrical introgression. These studies observed that large-effect mutations were more likely to contribute to genetic incompatibility but did not fully describe how the speed and direction of environmental change contributed to overall reproductive isolation, including both intrinsic and extrinsic isolation.

An alternative approach was proposed by Simon *et al*. (2018), who considered "tethered" random walks of different populations around a single environmental optimum, allowing the authors to predict the fitnesses of different hybrid types, but not exploring a history of adaptation and not allowing for different parental optima.

Here we assess how both the history of adaptation and the degree of environmental similarity between two populations impact the mean fitness of a variety of hybrid crosses (e.g., F_1, F_2, backcross to local, backcross to foreign parents) for both haploid and diploid species. Through simulations, we illustrate how the importance of ecological speciation varies, depending on the history of adaptation, the mean mutational size, and the cross considered. Our results emphasize how the nature of past selection – divergent or parallel – has a substantial effect on the mean fitness of hybrids as measured in different environments.

We also consider how the modularity of the genotype-phenotype relationship impacts the development of reproductive isolation under mutation-order speciation. To vary modularity, we investigate a generalized form of Fisher's geometric model (FGM), in which the level of pleiotropy can be tuned. The original FGM assumes that a mutation affects all traits under consideration (i.e., universal pleiotropy; fitness landscape is a single hypersphere). Here, we also consider a "multi-sphere model," where each mutation affects only one of several sets of trait values (modular pleiotropy, Welch and Waxman 2003; Chevin et al. 2010; Wagner and Zhang 2011). We expected a higher degree of parallel evolution, leading to less reproductive isolation, in cases where the environment changed in the same direction (affecting the same sphere) in different populations, but unexpectedly we found a non-monotonic relationship between the extent of speciation and the degree of modularity.

Finally, we explore the potential for hybrids to colonize new sites beyond the range of the parental species. Crosses between individuals from two adapted populations can produce a wide variety of hybrid genotypes, potentially allowing hybrids to survive beyond the environmental conditions in which parental genotypes can survive (Albertson and Kocher 2005). We thus explored the range of environments in which hybrids were more likely to establish than parental individuals, potentially contributing to hybrid speciation (i.e., without a change in ploidy: "homoploid hybrid speciation").

Overall, our work explores how the nature of environmental change and the

modularity of the genetic architecture influence the development of reproductive isolation, as measured in various hybrid crosses, and the potential for hybrid speciation.

Model

We first describe the fitness landscape in our model and then describe how we simulate the evolution of reproductive isolation.

Fitness landscape

Fisher's model assumes multivariate stabilizing selection around a single optimum. We extend this model by defining an individual's phenotype as *m* sets of *n*-dimensional vectors, where *m* is the number of spheres and *n* is the number of traits in each sphere. Specifically, the phenotype of an individual in the *i*th sphere is $\mathbf{z}_i = \{z_{i,1}, z_{i,2}, ..., z_{i,n}\}$, whose components $z_{i,j}$ are the phenotypic values for each trait. The fitness component based on the set of traits described by this sphere depends on the distance of the phenotype from the optimum $\mathbf{o}_i = \{o_{i,1}, o_{i,2}, ..., o_{i,n}\}$, measured as the Euclidean distance $\|\mathbf{z}_i - \mathbf{o}_i\| \equiv \sqrt{\sum_{j=1}^{n} (z_{i,j} - o_{i,j})^2}$. Assuming that an individual's relative fitness is calculated by considering fitness across all spheres in a multiplicative fashion, fitness is given by:

$$w(\mathbf{z}_1, \mathbf{z}_2, ..., \mathbf{z}_m) = \exp\left(-q \sum_{i=1}^{m} \|\mathbf{z}_i - \mathbf{o}_i\|^k\right), \qquad \text{(Eq. 1)}$$

where q sets the overall strength of selection and k determines the curvature of the fitness function. The parameter k corresponds to the degree of epistasis (Tenaillon 2014). It is worth noting that selection is assumed independent and equally strong on all $m \times n$ traits, for a given distance to the optimum (isotropic selection).

Each mutation additively shifts the phenotypic value relative to its present value. In the multi-sphere model, we assume that a mutation affects one, and only one, sphere, chosen at random. Once a sphere is chosen, the mutation affects all of the *n* traits in the sphere under consideration, in a random direction (isotropic mutation). While the trait axes can be defined to allow isotropy with respect to either selection or mutation (assuming a single optimum), it is not possible to do so for both. Nevertheless,

167 previous work exploring a non-isotropic FGM model has shown that the isotropic FGM
168 serves as a good approximation, in many cases, if we consider n to be an effective
169 number of dimensions (Waxman and Welch 2005; Martin and Lenormand 2006).

170 Let us denote the mutational change in the ith sphere as
171 $\Delta\mathbf{z}_i = \{\Delta z_{i,1}, \Delta z_{i,2}, ..., \Delta z_{i,n}\}$ for haploids or for homozygous diploids. We assume that
172 the mutational change in each trait is drawn independently from a standard normal
173 distribution, denoted as ξ_i (Hartl and Taubes 1998; Fraisse *et al*. 2016). The
174 mutational change of trait i is given by $\Delta z_i = r\xi_i / \sqrt{\sum_{i=1}^{n} \xi_i^2}$ where r is a known size to
175 constrain the magnitude of each mutation, drawn from a distribution, specifically from
176 an exponential distribution with mean λ (for alternative distributions, see discussion
177 in Poon & Otto 2000). The selection coefficient of the mutation is then expressed as
178 $s \equiv \frac{w(\mathbf{Z}+\Delta\mathbf{Z})}{w(\mathbf{Z})} - 1$, where $\mathbf{Z}+\Delta\mathbf{Z}$ is the phenotypic vector of a mutant individual
179 across all spheres. In diploids, the above describes the properties of homozygous
180 mutations. Heterozygous diploids are assumed to be shifted half as much in phenotype
181 space, $\Delta\mathbf{z}_i / 2$ (i.e., we assume additivity on a phenotypic scale). The dominance
182 coefficient for fitness is then defined as $h \equiv \left(\frac{w(\mathbf{Z}+\Delta\mathbf{Z}/2)}{w(\mathbf{Z})} - 1 \right) \Big/ s$.

183

184 ***Simulation methods***

185 We consider a species that is sexually-reproducing with non-overlapping generations.
186 The species is sub-divided into two finite populations, each comprising N
187 hermaphrodites with no migration between them (i.e., allopatry). Initially, these
188 populations are genetically identical, having just separated geographically. Genomes
189 may be haploid or diploid and are assumed to be large enough for each mutation to
190 occur at a unique site (i.e., infinite sites).

191 Mutations that affect fitness occur stochastically every generation, but we
192 assume that the mutation rate is quite low to keep the product of the rate and population
193 size much smaller than one. This condition allows us to assume that a population is
194 monomorphic most of the time (Kimura and Ohta 1969; Taylor *et al*. 2006). Thus, we
195 consider the fate of mutations one at a time (Orr 1998; Chevin *et al*. 2014). Each

mutation that arises reaches fixation within a single-population with probability $\frac{1-\exp(-2s)}{1-\exp(-2Ns)}$ in haploids and $\frac{\int_0^{\frac{1}{2N}} e^{-2Ns(2h-1)x(1-x)-2Nsx}dx}{\int_0^1 e^{-2Ns(2h-1)x(1-x)-2Nsx}dx}$ in diploids (Crow and Kimura 1970). Note that overdominance naturally arises, at least transiently, in diploid models of adaptation to a new optimum (Sellis et al. 2011). We assume that the population size is small enough that polymorphisms are sufficiently transient to be ignored, although this assumption is more tenuous in diploids with overdominance. To simplify the simulations, we track time in units of fixation events, where we randomly choose mutations and assign them to one or the other population, repeating until one fixes.

As the two populations accumulate mutations, they independently traverse the fitness landscapes in the two patches. While this necessarily leads to genetic divergence, the populations may remain similar phenotypically or may diverge initially and subsequently converge (or vice versa), depending on the optima in the two patches. To explore the impact of this process on reproductive isolation, we study the following three types of environmental scenarios:

(1) Adaptation to a fixed common optimum, shifted from the position of the initial population (to investigate mutation-order speciation).
(2) Adaptation to a common moving optimum (to investigate mutation-order speciation in a changing environment).
(3) Adaptation to different fixed optima (to investigate ecological speciation).

Let us define the vector of optima across all spheres as $\mathbf{O}=\{\mathbf{o}_1,\mathbf{o}_2,...,\mathbf{o}_m\}$. By assumption, the initial phenotype $\mathbf{Z}_0$ is the same in the two populations and set to the origin in all *m* spheres. Under scenario (1), adaptation proceeds from $\mathbf{Z}_0$ towards $\mathbf{O}$ in both patches. Under scenario (2), the optimum starts at $\mathbf{O}_S$ and moves to $\mathbf{O}_E$ in a linear fashion for a period of τ fixation events (summed over the two populations). Under scenario (3), adaptation proceeds towards $\mathbf{O}_A$ in patch A and towards $\mathbf{O}_B$ in patch B.

We measure the level of reproductive isolation between the two populations through crosses, generating F_1, F_2, and backcross (BC) hybrids. To generate F_1

227 individuals in the haploid case, for example, when there are x fixed mutants in patch A
228 and y fixed mutations in patch B, we randomly choose each mutation with a 50%
229 probability of being passed to each offspring, so that there are, on average, $(x+y)/2$
230 mutations in each hybrid. In the diploid case, all F_1 hybrids are identical and are
231 heterozygous for all x and y mutations. The phenotype of a hybrid individual is then
232 calculated as the sum of the mutational vectors, and its fitness is assessed in both
233 parental environments. This is repeated 1000 times for each hybrid type. FGM
234 simulations for adaptation and for producing hybrids were written in C++ and
235 *Mathematica*, respectively (to be deposited in Dryad).

236 We were also interested in the time course over which reproductive
237 incompatibilities developed. Whereas some models have assumed that all divergent
238 pairs of loci are equally likely to give rise to speciation barriers (Orr 1998), we
239 speculated that large-effect mutations that accumulate early during adaptation may
240 contribute disproportionately. For each population, we thus accumulated an equal
241 number of fixation events in two phases: the phase during which adaptation occurred
242 ("adaptation phase") and the phase during which the population moved randomly
243 around the optimum ("circling phase"). For simplicity, we defined the initial phase as
244 the time until the first mutation fixed with a negative selection coefficient. For scenario
245 (2) with a moving optimum, the initial phase was defined as the time until the first
246 mutation fixed with a negative selection coefficient after the optimum stopped moving,
247 as sometimes deleterious alleles fixed early on while the optimum was still close to the
248 initial phenotype. In addition, for modular pleiotropy, we assumed that the adaptation
249 phase continued until the first fixed allele with a negative selection coefficient within
250 the focal sphere in which the optimum had moved.

251 To translate the number of fixation events into a more biologically
252 meaningful time scale, we calculated the expected number of generations until
253 appearance and fixation of the next mutation and summed this quantity across the series
254 of mutations fixed. Given the mutation rate u, we first calculated the waiting time until
255 the appearance of the next "successful" mutation that would survive stochastic loss
256 while rare. This waiting time was assumed to be exponentially distributed with a rate of
257 events equal to the mutation rate, u (set as 10^{-5} throughout this paper) multiplied by
258 the number of haplotypes in the population ($c\,N$, where c = 1 for haploids and 2 for
259 diploids) times the average fixation probability, P. The latter varies depending on the

current distance of the population from the optimum and was determined by integrating P over the distribution of possible mutations for each state of the population. The mean waiting time of this exponential distribution is $1/(cNuP)$ generations. Then, we calculated the fixation time of the successful allele that was drawn, using the expected waiting time until fixation for a new mutation (Ewens 2000; Otto & Day 2007). Given the selection coefficient and the dominance coefficient of a mutation, the expected waiting time, conditional upon fixation, is approximately (Kimura 1980):

$$T = \int_0^1 \int_0^y \frac{2}{V(x)} e^{-2\int_x^y \frac{M(z)}{V(z)} dz} dxdy\,, \qquad \text{(Eq. 2)}$$

where M and V are the mean and variance of the change of mutation allele frequency p per generation. Those values are $M(p) = sp(1-p)$ and $V(p) = \frac{p(1-p)}{N}$ in haploids and $M(p) = p(1-p)\left[sp + h(1-2p)\right]$ and $V(p) = \frac{p(1-p)}{2N}$ in diploids. The expected waiting time until the next mutation appears and fixes then becomes $1/(cNuP)$ plus:

$$T = \int_0^1 \int_0^y \frac{2N}{x(1-x)} e^{-2Ns(y-x)} dxdy \qquad \text{(Eq. 3a)}$$

in haploids and

$$T = 4N \int_0^1 e^{-2Nsy^2 - 4Nhy(1-y)} \int_0^y \frac{e^{-2Nsx^2 + 4Nhx(1-x)}}{x(1-x)} dxdy \qquad \text{(Eq. 3b)}$$

in diploids, respectively.

Results

Evolutionary trajectory of adaptation

Under Fisher's geometric model (FGM), mutations have nearly a 50% chance of being beneficial when a population starts far from the optimum relative to the effect size of the mutation, but they are more likely to overshoot the optimum and less likely to fix once the population approaches the optimum (Fisher 1930; Kimura 1983). As a consequence, during the process of adaptation, the average phenotypic effect size of fixed mutations declines as populations become increasingly adapted (Figure 1; Orr 1998). When the distribution of mutations has a larger average magnitude, we find that the optimum is reached faster, as one might expect (Figure 1c). After nearing the

288 optimum, populations accumulate a combination of slightly deleterious and beneficial
289 mutations (inset to Figure 1b), resulting in a phase of mutation-selection-drift where the
290 populations stochastically move around the optimum through successive fixation
291 events.
292 After simulating a period of adaptation, we next performed crosses between
293 populations to determine how hybrid fitness depended on the nature of environmental
294 change, the mutation effect size, ploidy, and the modularity of pleiotropy. In these
295 simulations, we allowed the same total number of fixation events to occur in the initial
296 adaptation phase and in the second circling phase in each parental populations (allowing
297 each population to accumulate a different number of fixed mutations). Table S2 gives
298 the number of fixation events in each parental population and the corresponding
299 expected number of generations.
300
301 *Adaptation to a common optimum* – Figure 2 shows hybrid fitness after a period of
302 adaptation towards a common fixed optimum in (a) haploids and (b) diploids (for an
303 exploration of introgression effects, see Fraïsse *et al*., 2016). For the parameters
304 considered, substantial reproductive isolation is observed in all hybrids, with the
305 exception of diploid F_1s. Diploid F_1s are not yet recombinant but heterozygous at all
306 sites that differ between the parents. When parents near the same optimum are crossed
307 in the FGM, averaging their phenotype in the F_1 reduces the distance to the peak and
308 increases fitness relative to the parents, as discussed by Barton (2001), Fraïsse *et al*.
309 (2016), and Simon *et al*. (2018).
310 By contrast, all recombinant hybrids have reduced average fitness, relative to
311 the parents, reflecting the segregation load studied by Chevin et al. (2014). Importantly,
312 the incompatibility results primarily from the pleiotropic effects of mutations that
313 accumulate during adaptation and is not observed to any substantial degree when the
314 optimum remains at the origin, even with the same number of fixation events (Figure
315 S1).
316 The vast majority of the reproductive isolation that accumulated was during
317 the first adaptation phase when large-effect mutations were likely to fix. Considering
318 only these mutations, F_2 hybrid fitness, for example, was reduced below the optimum
319 by, on average, 0.72 in haploids and 0.74 in diploids. By contrast, F_2 hybrid fitness
320 remained much higher, 0.99 in haploids and 0.98 in diploids, when we add the same

321 number of mutations that occurred only during the circling phase to the optimum (see
322 Table S2 for the number of fixation events in each population).
323 During the period of adaptation, large mutations can become fixed, despite the
324 fact that they shift the phenotype substantially away from the origin in some directions,
325 as long as the average phenotypic distance to the optimum is shorter. In subsequent
326 generations, these negative pleiotropic side effects favor the fixation of compensatory
327 mutations that move the phenotype back toward the optimum. In recombinant hybrids,
328 however, these compensatory mutations are separated from the mutant backgrounds in
329 which they are favored, reducing fitness. Consequently, as expected, the fitness
330 reduction in hybrids is more severe when mutational effect sizes (and hence pleiotropic
331 side effects) are larger, on average (Figure 3).
332
333 *Adaptation to a common moving optimum* – The above simulations were repeated but
334 allowing the optimum to move more slowly towards its final position, $\mathbf{O}_E$. With a more
335 slowly moving optimum, large-effect mutations have a lower probability of fixation,
336 reducing the accumulation of negative pleiotropic side-effects. Consequently, we find
337 that much weaker reproductive isolation develops, with higher hybrid fitness, after a
338 period of slow environmental change, even when ultimately reaching the same optimum
339 (Figure 4).
340
341 *Adaptation to different optima* – In the next scenario, we simulated isolated populations
342 adapting to different fixed optima, assessing hybrid fitness in both parental
343 environments. The results are qualitatively different in diploids, and F_1 hybrids now
344 have low fitness within each environment, as their phenotype falls between the optima
345 of the two environments (Figure 5). The larger the angle between the two optima, the
346 lower the F_1 hybrid fitness. In addition, the fitness reduction in hybrids is more severe
347 when mutational effect sizes are larger (see sets of three adjacent points), but the effect
348 is smaller than the effect of the angle between the two environments (in diploids, much
349 smaller).
350 Backcross hybrids to the local parent, BC_L, now show much higher fitness
351 than backcross hybrids to the foreign parent, BC_F (Figure S3), a hallmark of ecological
352 speciation (Rundle and Whitlock 2001). The relative performance of the various hybrids
353 depends, however, on the angle between the two optima (compare Figure S3 with an

354 angle of $\pi/2$ to Figure S2 with $\pi/6$). As a measure of the importance of ecological
355 speciation, Rundle and Whitlock (2001) suggest calculating the fitness of BC_L minus
356 the fitness of BC_F, averaged over the two local environments, as this estimates the
357 strength of additive-by-environment interactions (AE). Indeed, AE falls from ~0.4-0.6
358 when the environments are far apart (an angle of $\pi/2$) to 0 when the environments are
359 identical (Figure 6a,b). Across the full range of angles, however, AE behaves
360 non-monotonically (Figure 6a,b), because the fitness of the local BC_L falls to zero when
361 the environments are very dissimilar, severely limiting the maximum value of AE. The
362 degree to which ecological speciation contributes to reproductive isolation may be
363 better captured by measuring AE relative to the maximum value it could take (i.e., AE
364 divided by the fitness of BC_L), which does rise monotonically with the degree of
365 environment difference (Figure 6c,d), although sample sizes would need to be sufficient
366 to avoid bias caused by measurement error in the denominator.
367
368 ***Impact of modularity***
369 We next investigated the degree to which modularity of the phenotype would affect the
370 development of reproductive incompatibilities between adapting populations. To
371 investigate different degrees of modular pleiotropy, we held the total number of
372 phenotypic dimensions constant (the number of spheres times the number of traits per
373 sphere = $m\ n$) but varied the number of spheres. To simplify the presentation, we
374 consider only F_1 hybrids in haploid simulations. Our prediction was that we would
375 observe less negative pleiotropy when the phenotype was more modular, leading to less
376 hybrid breakdown, but this was not the case (Figure 7a). Instead, reproductive isolation
377 showed a non-monotonic pattern, with more hybrid breakdown in the fully pleiotropic
378 model (m = 1) and in the model with no pleiotropy (n = 1) than with intermediate levels
379 of pleiotropy.
380 To understand this counter-intuitive result, we investigated how the genes
381 contributing to hybrid breakdown accumulated over time. Relatively little contribution
382 came from mutations accumulating during the circling phase, so we sub-divided the
383 mutations accumulated during the adaptation phase into two groups: the first 50% of
384 mutations that fixed and the second 50% of mutations that fixed. With more modular
385 genetic networks (m larger; Figure 7b), mutations fixed during the first half of
386 adaptation were more likely to work well together, increasing mean hybrid fitness as we

had expected. When the environmental change occurs in a module with few traits (low n), mutations that fix in one population are more likely to point towards the optimum and be beneficial in another population. By contrast, as the population approached the optimum during the second half of the adaptation phase, mutations were increasingly likely to arise in different modules, by chance, in different populations (recall that the circling phase was defined to start only after a deleterious mutation arose in the module experiencing environmental change). Consequently, the more modules, the less likely mutations in different populations would compensate for one another, so that decreased hybrid fitness was observed with more modularity (Figure 7c). Thus, the role of modularity in speciation had opposite effects during early and rapid periods of adaptation, where reproductive isolation developed faster in more highly pleiotropic systems, versus during periods of relatively slow adaptation, where reproductive isolation developed faster in more modular systems.

Homoploid hybrid speciation

Finally, we investigated the possibility of homoploid hybrid speciation using hybrids generated between two parental populations. The fitness of F_1 hybrid haploids was assessed in a new environment with optimum $\mathbf{O}_P$, representing a potential site for colonization. The probability of establishment in a site for any genotype, P_e, was determined by the branching process approximation $1-P_e = e^{-wbP_e}$, assuming a Poisson number of offspring with mean equal to the genotypic fitness w times the average reproductive capacity, b, of an individual with full fitness of w=1. We repeated this calculation for 1000 hybrids and averaged P_e to get the expected establishment probability. We then measured the relative establishment probability of hybrids to the average establishment probability of the two parental genotypes.

Figure 8 illustrates the relative colonization success of hybrid haploids, as a function of the phenotypic optimum in the new environment. Considering first the case where parents have adapted to the same environmental optimum (Figure 8a), hybrids are more likely to colonize substantially different environments than the parental populations when hybrid variance is large (orange halo). This effect is minimal in the circling phase (Figure 8b) but rises after a period of adaptation (Figure 8a), indicating that hybrid speciation is more likely when parental populations have experienced environmental change than when they have experienced a stable environment. In

420 addition, when the parental populations adapt to different environments, hybrids
421 become much better at colonizing new environments that fall between the optima of the
422 parental populations (Figure 8c,d). Homozygous diploid F_2s behave similarly, but the
423 establishment probability of diploids in general would have to account for segregation
424 variance after colonization, which was not explored.
425
426 **Discussion**
427 We used a simple model of optimizing selection on multiple traits ("Fisher's geometric
428 model") to explore speciation in the face of environmental change. Because the path of
429 adaptation in Fisher's geometric model varies among populations evolving in allopatry,
430 genetic crosses between populations yield mis-matched combinations of adaptive
431 mutations, producing hybrid offspring of lower fitness (post-zygotic isolation). Our
432 main conclusion from this model is that periods of adaptation are likely engines of
433 speciation for allopatric populations, whether the populations are adapting to similar
434 environmental changes ("mutation-order speciation"; Figure 3) or different ones
435 ("ecological speciation"; Figure 5). Reproductive incompatibilities were strongest when
436 large-effect mutations could accumulate, i.e., during times of major environmental
437 change, which challenges the notion that all genetic substitutions are equally likely to
438 generate reproductive incompatibilities.
439 We also explored the relative importance of mutation-order speciation versus
440 ecological speciation by comparing the fitness of different hybrid crosses. Rundle and
441 Whitlock (2001) showed that the contribution of ecological speciation could be captured
442 by the additive-by-environment interaction (AE), estimated from the fitness of
443 individuals backcrossed to the local population (BC_L) minus the fitness of individuals
444 backcrossed to a foreign population (BC_F). Only under ecological speciation are these
445 backcross fitnesses expected to differ. We find that this AE measure does indeed rise
446 with the angle of environmental optima between two evolving populations (measured
447 here relative to their ancestral origin), but only when that angle was small. With larger
448 environmental differences, the fitness of even the local backcrossed individuals (BC_L)
449 could be very low, leading AE to drop (Figure 6a,b). As a correction for this
450 non-monotonic behavior, we instead investigated a new measure of the importance of
451 ecological speciation, dividing AE by its maximum expected value (BC_L), which we
452 found does rise with the angle of environmental differences in our study (Figure 6c,d).

We also considered how the modularity of the genotype-phenotype relationship impacted the development of reproductive isolation under mutation-order speciation. With a more modular genetic architecture, allopatric populations experiencing the same environmental change are more likely to accumulate mutations that are compatible, because the negative pleiotropic effects of adaptive mutations are constrained within the module affected by the environmental change. Thus, we expected a higher degree of parallel evolution, leading to less reproductive isolation, in cases where the environment changed in the same direction in different populations. Unexpectedly, we found a non-monotonic relationship between the extent of reproductive isolation and the degree of modularity (Figure 7). By separating out the first half of mutations fixed during the early and rapid phase of adaptation from the latter half of mutations fixed during the adaptation phase, we were able to verify that reproductive isolation is less likely to develop early on during adaptation in more modular systems, but this is counteracted by a greater chance that mutations generate reproductive isolation during later phases of adaptation as populations more slowly approach the optimum. The key difference between these phases was whether fixed mutations tended to fix primarily in the same module – the one responding to the shifting environment – or in different modules. Once the populations are near the optimum, different populations tended to fix mutations and compensatory mutations in different modules, substantially increasing the chance of hybrid breakdown when crossed.

In addition, we explored the conditions conducive to homoploid hybrid speciation. Because hybrids can vary in phenotype beyond the range of parental populations, hybrids can successfully colonize environments inaccessible to parental populations, potentially contributing to homoploid hybrid speciation (Gross and Rieseberg 2005). Importantly, we found that hybrid speciation was especially likely when the parental populations had undergone a period of adaptation in allopatry (Figure 8). The parents were then more likely to differ by large-effect mutations, allowing hybrid genotypes to vary more broadly in phenotype and succeed in more extreme environments. We thus predict that periods of adaptation by the parental forms may be particularly conducive to subsequent homoploid hybrid speciation.

Caveats and future directions

We made several simplifying assumptions in this study that warrant more exploration in future work. For one, we assumed that populations are largely monomorphic, punctuated in time by the fixation of new mutations. This assumption breaks down in larger populations (N) or in environments with a larger number of potential mutations (higher u; a standing genetic variation, Thompson et al. 2019). Thus, future work should consider the development of reproductive isolation allowing for polymorphic alleles at multiple loci throughout the genome. Relaxing the assumption of monomorphism is particularly important for diploid populations, because large effect mutations often arise that overshoot the optimum, leading to overdominance that maintains polymorphism (Sellis et al. 2011).

Our understanding of the role of rapid adaptation and the fixation of large-effect mutations to speciation would also benefit from exploring other forms of selection beyond the simple Fisherian geometric model considered here. With multiple optima or other complex fitness landscapes (e.g., the "holey adaptive landscape" of Gavrilets 1997), mutation-order speciation is thought to be even more likely, as populations may move to different points on the fitness landscape, depending on the order in which mutations arise (Gavrilets 2004). Nevertheless, we conjuecture that the degree of reproductive isolation may still be stronger when initially further away from the peaks of the fitness surface, because large-effect mutations may then be more likely to fix in different directions in allopatric populations, relative to the small-effect mutations providing slight improvements in fitness near a local optimum.

As an example of speciation across a more complex fitness landscape, Benkman (2003) showed that the fitness surface of red crossbills feeding on cones from different coniferous tree species displayed different peaks, associated with distinct call types, with both ridges of relatively high fitness and deep fitness valleys. Although not explored in this paper, the combination of fitness ridges with deep valleys might facilitate reproductive isolation by allowing large-effect mutations that reach different points along the ridge and that, when combined, cause hybrid phenotypes to exhibit low fitness.

Fluctuating selection could also contribute to the accumulation of large-effect mutations and be a potent driver of speciation (see, e.g, Barton 2001; Chevin et al. 2014; Fraïsse et al. 2016). For example, beak phenotypes of the medium ground finch *Geospiza fortis* on Galapagos have experienced selection that fluctuates between life

stages, years and generations (Price and Grant 1984; Grant and Grant 2008). Stabilizing selection with a fluctuating optimum allows the population to accumulate relatively large mutations, which contribute disproportionately to the accumulation of reproductive isolation.

In conclusion, our work shows that the tempo of speciation does not tick at a steady rate. Rather, reproductive isolation between allopatric populations should rise faster after bouts of rapid environmental change. In our simulations, crossing the few large-effect mutations that arose during bouts of rapid adaptation caused more hybrid breakdown than combining many small-effect mutations, whose effects tended to cancel (see also eq. 3 in Chevin et al. 2014). These results help explain the surprisingly rapid appearance of reproductive isolation during short-term experimental evolution studies in the lab (e.g., Dettman et al. 2007, 2008; Kvitek and Sherlock 2011; Chou et al. 2014; Ono et al. 2017), which tend to impose strong selection, despite the fact that the world has not evolved into an infinite variety of species.

533 **Author contributions**

534 RY and SPO designed the study; RY developed the computer simulation code and
535 conducted analyses in consultation with SPO; RY and SPO wrote the manuscript.

536

537 **Data accessibility**

538 All code necessary to repeat the analysis described in this study have been made
539 available. C++ source codes of our simulation models for adaptation process,
540 *Mathematica* (version 11.2.0.0) codes for calculating hybrids genotypes and fitnesses, R
541 (version 3.5.1) scripts that we used to produce figures, and simulation results in this
542 paper will be available from the Dryad Digital Repository. For now, these are hosted on
543 Github (https://github.com/ryamaguchi0731/FGM-master).

544

545 **Acknowledgements**

546 This work was supported by funding from the Japanese Society for the Promotion of
547 Science (Research Fellowship for Young Scientists, DC1-14J02775 and PD-17J01380,
548 to RY) and from the Natural Sciences and Engineering Research Council of Canada
549 (RGPIN-2016-03711 to SPO). We thank the following people for their helpful
550 comments on previous drafts of the manuscript: Yoh Iwasa, Matt Osmond and Ken
551 Thompson. We are grateful to Matt Osmond for suggesting the normalization of AE by
552 BC_L as a more informative measure of ecological speciation.

Literature Cited

1. Albertson, R. C., & Kocher, T. D. (2005). Genetic architecture sets limits on transgressive segregation in hybrid cichlid fishes. *Evolution*, *59*(3), 686-690.
2. Barton, N. H. (2001). The role of hybridization in evolution. *Molecular Ecology*, *10*(3), 551-568.
3. Benkman, C. W. (2003). Divergent selection drives the adaptive radiation of crossbills. *Evolution*, *57*(5), 1176-1181.
4. Chevin, L. M., Decorzent, G., & Lenormand, T. (2014). Niche dimensionality and the genetics of ecological speciation. *Evolution*, *68*(5), 1244-1256.
5. Chevin, L. M., Martin, G., & Lenormand, T. (2010). Fisher's model and the genomics of adaptation: restricted pleiotropy, heterogenous mutation, and parallel evolution. *Evolution*, *64*(11), 3213-3231.
6. Chou, H. H., Delaney, N. F., Draghi, J. A., & Marx, C. J. (2014). Mapping the fitness landscape of gene expression uncovers the cause of antagonism and sign epistasis between adaptive mutations. *PLoS genetics*, *10*(2), e1004149.
7. Crow, J. F., & Kimura, M. (1970). An introduction to population genetics theory. *An introduction to population genetics theory*.
8. Dettman, J. R., Anderson, J. B., & Kohn, L. M. (2008). Divergent adaptation promotes reproductive isolation among experimental populations of the filamentous fungus Neurospora. *BMC Evolutionary Biology*, *8*(1), 35.
9. Dettman, J. R., Sirjusingh, C., Kohn, L. M., & Anderson, J. B. (2007). Incipient speciation by divergent adaptation and antagonistic epistasis in yeast. *Nature*, *447*(7144), 585-588.
10. Ewens, W. J. (2000). *Mathematical population genetics 1: theoretical introduction*. Springer.
11. Fisher, R. A. (1930). *The genetical theory of natural selection*. Clarendon Press, Oxford, UK.
12. Fraïsse, C., Gunnarsson, P. A., Roze, D., Bierne, N., & Welch, J. J. (2016). The genetics of speciation: Insights from Fisher's geometric model. *Evolution*, *70*(7), 1450-1464.
13. Gavrilets, S. (1997). Evolution and speciation on holey adaptive landscapes. *Trends in ecology & evolution*, *12*(8), 307-312.
14. Gavrilets, S. (2004). *Fitness landscapes and the origin of species (MPB-41)* (Vol.

586 41). Princeton University Press.
587 15. Grant, P. R., & Grant, B. R. (2008). *How and why species multiply: the radiation of*
588 *Darwin's finches*. Princeton University Press.
589 16. Gross, B. L., & Rieseberg, L. H. (2004). The ecological genetics of homoploid
590 hybrid speciation. *Journal of heredity*, *96*(3), 241-252.
591 17. Hartl, D. L., & Taubes, C. H. (1998). Towards a theory of evolutionary
592 adaptation. *Genetica*, *102*, 525-533.
593 18. Kimura, M. (1980). Average time until fixation of a mutant allele in a finite
594 population under continued mutation pressure: Studies by analytical, numerical,
595 and pseudo-sampling methods. *Proceedings of the National Academy of*
596 *Sciences*, *77*(1), 522-526.
597 19. Kimura, M. (1983). *The neutral theory of molecular evolution*. Cambridge
598 University Press.
599 20. Kimura, M., & Ohta, T. (1969). The average number of generations until fixation
600 of a mutant gene in a finite population. *Genetics*, *61*(3), 763.
601 21. Kvitek, D. J., & Sherlock, G. (2011). Reciprocal sign epistasis between frequently
602 experimentally evolved adaptive mutations causes a rugged fitness
603 landscape. *PLoS genetics*, *7*(4), e1002056.
604 22. Mani, G. S., & Clarke, B. C. (1990). Mutational order: a major stochastic process
605 in evolution. *Proceedings of the Royal Society of London B: Biological*
606 *Sciences*, *240*(1297), 29-37.
607 23. Martin, G., & Lenormand, T. (2006). A general multivariate extension of Fisher's
608 geometrical model and the distribution of mutation fitness effects across
609 species. *Evolution*, *60*(5), 893-907.
610 24. Mendelson, T. C., Martin, M. D., & Flaxman, S. M. (2014). Mutation-order
611 divergence by sexual selection: diversification of sexual signals in similar
612 environments as a first step in speciation. *Ecology letters*, *17*(9), 1053-1066.
613 25. Ono, J., Gerstein, A. C., & Otto, S. P. (2017). Widespread genetic incompatibilities
614 between first-step mutations during parallel adaptation of Saccharomyces
615 cerevisiae to a common environment. *PLoS biology*, *15*(1), e1002591.
616 26. Orr, H. A. (1998). The population genetics of adaptation: the distribution of factors
617 fixed during adaptive evolution. *Evolution*, *52*(4), 935-949.
618 27. Otto, S. P., & Day, T. (2007). *A biologist's guide to mathematical modeling in*

ecology and evolution. Princeton University Press.

28. Poon, A., & Otto, S. P. (2000). Compensating for our load of mutations: freezing the meltdown of small populations. *Evolution*, *54*(5), 1467-1479.
29. Price, T. D., & Grant, P. R. (1984). Life history traits and natural selection for small body size in a population of Darwin's finches. *Evolution*, *38*(3), 483-494.
30. Rundle, H. D., & Whitlock, M. C. (2001). A genetic interpretation of ecologically dependent isolation. *Evolution*, *55*(1), 198-201.
31. Schluter, D. (2000). *The ecology of adaptive radiation*. OUP Oxford.
32. Schluter, D. (2009). Evidence for ecological speciation and its alternative. *Science*, *323*(5915), 737-741.
33. Schluter, D., & Conte, G. L. (2009). Genetics and ecological speciation. *Proceedings of the National Academy of Sciences*, *106*, 9955-9962.
34. Sellis, D., Callahan, B. J., Petrov, D. A., & Messer, P. W. (2011). Heterozygote advantage as a natural consequence of adaptation in diploids. *Proceedings of the National Academy of Sciences*, *108*(51), 20666-20671.
35. Simon, A., Bierne, N., & Welch, J. J. (2018). Coadapted genomes and selection on hybrids: Fisher's geometric model explains a variety of empirical patterns. *Evolution Letters*, *2*(5), 472-498.
36. Taylor, C., Iwasa, Y., & Nowak, M. A. (2006). A symmetry of fixation times in evoultionary dynamics. *Journal of theoretical biology*, *243*(2), 245-251.
37. Tenaillon, O. (2014). The utility of Fisher's geometric model in evolutionary genetics. *Annual review of ecology, evolution, and systematics*, *45*, 179-201.
38. Thompson, K. A., Osmond, M. M. and Schluter, D. (2019). Parallel genetic evolution and speciation from standing variation. *Evolution Letters*, doi:10.1002/evl3.106.
39. Wagner, G. P., & Zhang, J. (2011). The pleiotropic structure of the genotype–phenotype map: the evolvability of complex organisms. *Nature Reviews Genetics*, *12*(3), 204-213.
40. Welch, J. J., & Waxman, D. (2003). Modularity and the cost of complexity. *Evolution*, 57(8), 1723-1734.
41. Waxman, D., & Welch, J. J. (2005). Fisher's microscope and Haldane's ellipse. *The American Naturalist*, *166*(4), 447-457.

Table 1. Notation used. Default values are given in square brackets, except where noted in the text.

Notation	Description
m	Number of spheres [1]
n	Number of traits in each sphere [10]
$\mathbf{z}_i = \{z_{i,1}, z_{i,2}, \ldots, z_{i,n}\}$	Phenotype in the *i*th sphere
$\mathbf{o}_i = \{o_{i,1}, o_{i,2}, \ldots, o_{i,n}\}$	Optimum phenotype in the *i*th sphere
$w(\mathbf{z}_1, \mathbf{z}_2, \ldots, \mathbf{z}_m)$	Individual's relative fitness
q	Parameter translating the phenotypic distance from the optimum into the strength of selection [1]
k	Degree of epistasis [2]
$\mathbf{Z} = \{\mathbf{z}_1, \mathbf{z}_2, \ldots, \mathbf{z}_m\}$	Vector of phenotype sets of all spheres. $\mathbf{Z}_I$ is an initial condition
r	Mutation size, drawn from an exponential distribution with mean λ
ξ_j	Random number drawn from a standard normal distribution
$\Delta\mathbf{z}_i = \{\Delta z_{i,1}, \Delta z_{i,2}, \ldots, \Delta z_{i,n}\}$	Phenotypic change due to mutation in the *i*th sphere
$\Delta\mathbf{Z} = \{\Delta\mathbf{z}_1, \Delta\mathbf{z}_2, \ldots, \Delta\mathbf{z}_m\}$	Vector of mutational effects across all spheres
s	Selection coefficient
h	Measure of dominance
N	Number of individuals in a population [2000]
c	Ploidy level [1 for haploids, 2 for diploids]
u	Mutation rate [10^{-5}]
b	Number of offspring per individual of maximum fitness when calculating establishment probability [5]
$\mathbf{O} = \{\mathbf{o}_1, \mathbf{o}_2, \ldots, \mathbf{o}_m\}$	Vector describing the optimal phenotype across all sets of spheres

Table S1. The location of the environmental optima.

Angle between two optima	**Population 1**	**Population 2**	**Distance from Z_0 to O**
0	{2,0,0,0,0,0,0,0,0,0}	{2,0,0,0,0,0,0,0,0,0}	**2**
$\pi/6$	$\{-\sqrt{2-\sqrt{3}}, -\sqrt{2+\sqrt{3}},$ 0,0,0,0,0,0,0,0}	$\{\sqrt{2-\sqrt{3}}, -\sqrt{2+\sqrt{3}},$ 0,0,0,0,0,0,0,0}	**2**
$\pi/4$	$\{-\sqrt{2-\sqrt{2}}, -\sqrt{2+\sqrt{2}},$ 0,0,0,0,0,0,0,0}	$\{\sqrt{2-\sqrt{2}}, -\sqrt{2+\sqrt{2}},$ 0,0,0,0,0,0,0,0}	**2**
$\pi/2$	$\{-\sqrt{2}, -\sqrt{2},$ 0,0,0,0,0,0,0,0}	$\{\sqrt{2}, -\sqrt{2},$ 0,0,0,0,0,0,0,0}	**2**
π	{-2,0,0,0,0,0,0,0,0,0}	{2,0,0,0,0,0,0,0,0,0}	**2**

Vector angle is defined as $\mathrm{Arccos}\left[\frac{a \cdot b}{||a||\ ||b||}\right]$ where *a* and *b* are different vectors.

656 Table S2. Number of fixation events tracked within the parental populations P_1 and P_2
657 and the corresponding number of generations, based on the expected waiting time until
658 fixation. In each population, we tracked the same total number of fixations events
659 during the adaptation phase and the circling phase (e.g., 92 for P_1 and 88 for P_2 in each
660 phase for the first set of simulations).

Figure number & Population		**Total fixations**	**Number of generations**	**% of time in adaptation phase**
Figure 2, S1, 8a & 8b	P_1	184	2.31×10^7	8.32
(Haploid)	P_2	176	1.86×10^7	3.89
Figure 2 & S1	P_1	204	6.73×10^7	4.99
(Diploid)	P_2	184	5.72×10^7	2.75
Figure 3 & S3	P_1	159.52 ± 2.95	$1.85\times10^7 \pm 6.14\times10^5$	5.94 ± 0.38
(Haploid, $\lambda = 0.04$)	P_2	153.12 ± 4.45	$1.74\times10^7 \pm 7.54\times10^5$	7.15 ± 1.12
Figure 3	P_1	99.20 ± 1.98	$1.94\times10^7 \pm 6.17\times10^5$	5.99 ± 0.41
(Haploid, $\lambda = 0.08$)	P_2	98.44 ± 2.38	$1.86\times10^7 \pm 8.81\times10^5$	6.21 ± 0.46
Figure 3	P_1	83.44 ± 1.87	$2.25\times10^7 \pm 8.37\times10^5$	5.79 ± 0.43
(Haploid, $\lambda = 0.12$)	P_2	83.40 ± 1.44	$2.36\times10^7 \pm 6.63\times10^5$	7.03 ± 0.48
Figure 3 & S3	P_1	183.04 ± 2.93	$5.69\times10^7 \pm 1.73\times10^6$	3.86 ± 0.25
(Diploid, $\lambda = 0.04$)	P_2	181.48 ± 4.79	$5.36\times10^7 \pm 2.73\times10^6$	5.55 ± 1.01
Figure 3	P_1	133.08 ± 2.99	$1.11\times10^8 \pm 8.62\times10^6$	6.07 ± 1.97
(Diploid, $\lambda = 0.08$)	P_2	128.60 ± 4.91	$1.06\times10^8 \pm 5.79\times10^6$	6.40 ± 2.12
Figure 3	P_1	111.88 ± 2.31	$1.26\times10^8 \pm 1.28\times10^6$	5.68 ± 1.99
(Diploid, $\lambda = 0.12$)	P_2	112.56 ± 1.61	$1.30\times10^8 \pm 3.71\times10^6$	5.97 ± 1.98
Figure 4	P_1	222.36 ± 1.88	$3.05\times10^7 \pm 4.08\times10^5$	17.8 ± 0.51
(Haploid, slow)	P_2	216.20 ± 1.68	$2.97\times10^7 \pm 4.41\times10^5$	17.4 ± 0.48
Figure 4	P_1	166.32 ± 2.67	$2.02\times10^7 \pm 4.94\times10^5$	9.46 ± 0.27
(Haploid, medium)	P_2	166.12 ± 2.05	$2.02\times10^7 \pm 4.40\times10^5$	9.87 ± 0.33
Figure 4	P_1	155.24 ± 3.52	$1.79\times10^7 \pm 6.42\times10^5$	7.64 ± 1.31
(Haploid, fast)	P_2	158.22 ± 3.23	$1.78\times10^7 \pm 6.32\times10^5$	6.34 ± 0.31
Figure 4	P_1	215.12 ± 1.82	$8.02\times10^7 \pm 1.05\times10^6$	18.1 ± 0.70
(Diploid, slow)	P_2	216.64 ± 1.78	$8.11\times10^7 \pm 1.16\times10^6$	17.0 ± 0.67

Figure 4	P_1	180.04 ± 3.08	$5.83\times10^7 \pm 1.87\times10^6$	8.06 ± 0.29
(Diploid, medium)	P_2	170.12 ± 2.88	$5.41\times10^7 \pm 1.61\times10^6$	7.91 ± 0.34
Figure 4	P_1	177.68 ± 4.70	$5.47\times10^7 \pm 2.38\times10^6$	7.52 ± 1.74
(Diploid, fast)	P_2	177.88 ± 4.11	$5.66\times10^7 \pm 2.34\times10^6$	6.69 ± 1.12
Figure 5, 8c & S3	P_1	154.24 ± 3.84	$1.71\times10^7 \pm 7.37\times10^5$	5.83 ± 0.64
(Haploid, $\pi/6$,	P_2	158.28 ± 3.48	$1.78\times10^7 \pm 6.54\times10^5$	5.90 ± 0.40
$\lambda = 0.04$)				
Figure 5	P_1	101.36 ± 1.70	$1.92\times10^7 \pm 5.28\times10^5$	5.46 ± 0.41
(Haploid, $\pi/6$,	P_2	100.36 ± 2.75	$1.91\times10^7 \pm 7.88\times10^5$	6.30 ± 0.85
$\lambda = 0.08$)				
Figure 5	P_1	80.28 ± 1.52	$2.24\times10^7 \pm 6.07\times10^5$	7.36 ± 0.51
(Haploid, $\pi/6$,	P_2	82.48 ± 1.70	$2.19\times10^7 \pm 7.84\times10^5$	6.29 ± 0.63
$\lambda = 0.12$)				
Figure 5, 8d & S3	P_1	155.20 ± 2.81	$1.78\times10^7 \pm 5.35\times10^5$	5.48 ± 0.33
(Haploid, $\pi/4$,	P_2	153.26 ± 3.85	$1.77\times10^7 \pm 6.03\times10^5$	6.70 ± 0.88
$\lambda = 0.04$)				
Figure 5	P_1	103.24 ± 2.21	$2.06\times10^7 \pm 7.01\times10^5$	6.15 ± 0.42
(Haploid, $\pi/4$,	P_2	106.96 ± 2.31	$2.14\times10^7 \pm 6.42\times10^5$	6.61 ± 0.47
$\lambda = 0.08$)				
Figure 5	P_1	81.72 ± 1.84	$2.26\times10^7 \pm 8.27\times10^5$	6.77 ± 0.48
(Haploid, $\pi/4$,	P_2	85.20 ± 1.78	$2.46\times10^7 \pm 7.65\times10^5$	7.93 ± 0.58
$\lambda = 0.12$)				
Figure 5 & S3	P_1	156.88 ± 2.45	$1.80\times10^7 \pm 4.57\times10^5$	6.05 ± 0.36
(Haploid, $\pi/2$,	P_2	149.96 ± 3.17	$1.66\times10^7 \pm 6.31\times10^5$	5.10 ± 0.26
$\lambda = 0.04$)				
Figure 5	P_1	101.60 ± 2.10	$1.99\times10^7 \pm 6.31\times10^5$	6.75 ± 0.39
(Haploid, $\pi/2$,	P_2	101.44 ± 2.68	$1.99\times10^7 \pm 8.18\times10^5$	7.24 ± 0.63
$\lambda = 0.08$)				
Figure 5	P_1	83.52 ± 1.76	$2.38\times10^7 \pm 8.53\times10^5$	7.97 ± 0.59
(Haploid, $\pi/2$,	P_2	81.64 ± 1.76	$2.29\times10^7 \pm 7.79\times10^5$	7.05 ± 0.50
$\lambda = 0.12$)				

Figure 5 & S3 (Diploid, $\pi/6$, $\lambda = 0.04$)	P_1	189.32 ± 2.88	$6.02\times10^7 \pm 1.57\times10^6$	4.70 ± 0.30
	P_2	175.08 ± 5.62	$5.40\times10^7 \pm 2.53\times10^6$	6.67 ± 1.58
Figure 5 (Diploid, $\pi/6$, $\lambda = 0.08$)	P_1	134.12 ± 2.56	$1.14\times10^8 \pm 3.81\times10^6$	4.09 ± 0.73
	P_2	133.56 ± 2.30	$1.24\times10^8 \pm 3.42\times10^6$	3.45 ± 0.44
Figure 5 (Diploid, $\pi/6$, $\lambda = 0.12$)	P_1	111.92 ± 2.19	$1.29\times10^8 \pm 4.47\times10^6$	3.65 ± 0.93
	P_2	109.80 ± 2.25	$1.23\times10^8 \pm 4.31\times10^6$	4.79 ± 0.79
Figure 5 & S3 (Diploid, $\pi/4$, $\lambda = 0.04$)	P_1	188.16 ± 4.86	$5.90\times10^7 \pm 2.23\times10^6$	5.34 ± 0.82
	P_2	185.28 ± 3.94	$5.78\times10^7 \pm 1.79\times10^6$	5.05 ± 1.01
Figure 5 (Diploid, $\pi/4$, $\lambda = 0.08$)	P_1	138.08 ± 2.61	$1.19\times10^8 \pm 3.99\times10^6$	3.84 ± 0.40
	P_2	138.28 ± 2.31	$1.20\times10^8 \pm 3.45\times10^6$	4.31 ± 0.45
Figure 5 (Diploid, $\pi/4$, $\lambda = 0.12$)	P_1	110.88 ± 2.75	$1.22\times10^8 \pm 5.33\times10^6$	3.49 ± 0.71
	P_2	115.72 ± 1.60	$1.31\times10^8 \pm 4.04\times10^6$	3.13 ± 0.49
Figure 5 & S3 (Diploid, $\pi/2$, $\lambda = 0.04$)	P_1	186.06 ± 3.25	$5.82\times10^7 \pm 1.75\times10^6$	3.92 ± 0.26
	P_2	190.88 ± 3.69	$5.80\times10^7 \pm 1.99\times10^6$	4.08 ± 0.25
Figure 5 (Diploid, $\pi/2$, $\lambda = 0.08$)	P_1	133.56 ± 2.68	$1.15\times10^8 \pm 4.08\times10^6$	3.79 ± 0.47
	P_2	138.88 ± 3.16	$1.15\times10^8 \pm 4.30\times10^6$	4.73 ± 0.88
Figure 5 (Diploid, $\pi/2$, $\lambda = 0.12$)	P_1	116.92 ± 1.83	$1.38\times10^8 \pm 4.19\times10^6$	3.84 ± 0.45
	P_2	112.16 ± 1.87	$1.27\times10^8 \pm 4.25\times10^6$	3.55 ± 0.55
Figure S3 (Haploid)	P_1	144	1.19×10^7	2.59
	P_2	168	2.02×10^7	4.07
Figure S3 (Diploid)	P_1	188	5.23×10^7	2.98
	P_2	202	6.14×10^7	4.45

Figure 7	P_1	168.17 ± 4.56	$1.67\times10^7 \pm 2.99\times10^5$	9.81 ± 3.48
(1, 10)	P_2	166.64 ± 3.07	$1.77\times10^7 \pm 5.15\times10^5$	4.40 ± 1.74
Figure 7	P_1	133.56 ± 3.47	$2.97\times10^7 \pm 1.59\times10^6$	26.44 ± 1.42
(2, 5)	P_2	128.76 ± 3.06	$2.73\times10^7 \pm 1.15\times10^6$	25.09 ± 1.05
Figure 7	P_1	119.88 ± 5.84	$3.33\times10^7 \pm 2.54\times10^6$	43.17 ± 0.99
(5, 2)	P_2	114.92 ± 5.11	$3.04\times10^7 \pm 1.81\times10^6$	43.47 ± 1.05
Figure 7	P_1	138.36 ± 8.12	$4.09\times10^7 \pm 2.81\times10^6$	47.76 ± 0.90
(10, 1)	P_2	133.84 ± 8.35	$4.64\times10^7 \pm 5.36\times10^6$	46.31 ± 1.44
Figure S2	P_1	122	1.24×10^7	2.84
(Haploid)	P_2	138	1.52×10^7	3.44
Figure S2	P_1	166	4.26×10^7	1.80
(Diploid)	P_2	196	5.64×10^7	4.77
Figure 6	P_1	147.32 ± 3.41	$1.75\times10^7 \pm 5.24\times10^5$	6.00 ± 0.83
(Haploid, π)	P_2	151.13 ± 4.42	$1.78\times10^7 \pm 6.19\times10^5$	7.02 ± 1.06
Figure 6	P_1	187.72 ± 3.91	$5.81\times10^7 \pm 2.76\times10^6$	4.68 ± 0.98
(Diploid, π)	P_2	182.84 ± 3.80	$5.33\times10^7 \pm 1.62\times10^6$	4.19 ± 0.37

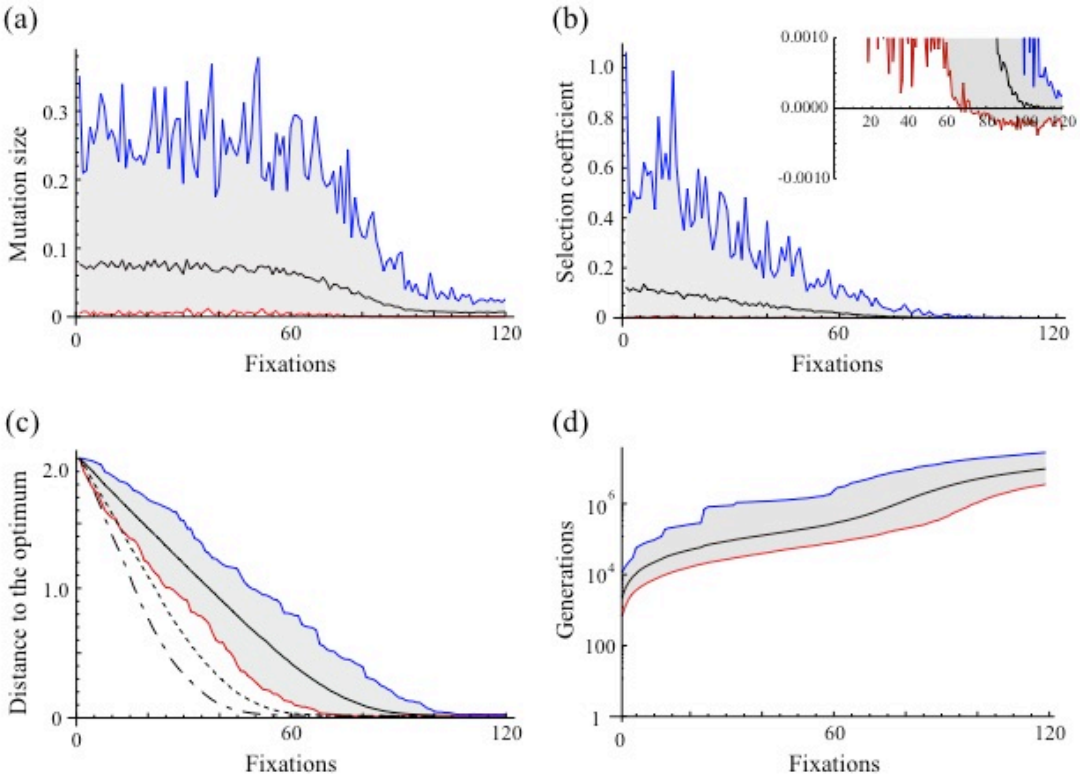

Figure 1. Trajectories within haploid simulations of (a) phenotypic effect size among fixed mutations, (b) selection coefficient, (c) distance to the optimum, and (d) time in units of generations versus the number of fixation events. Blue, red, and black represent maximum, minimum, and mean, respectively. Selection coefficients are positive in the first "adaptation phase" (taking, on average, 86.9 fixation events) but are more often negative in the second "circling phase" (inset to b). In (c), mutations are drawn from an exponential distribution with $\lambda = 0.04$ (right solid line), 0.08 (center dashed line), and 0.12 (left dashed-dotted line). All other panels set $\lambda = 0.04$. 100 simulations were run for each parameter set. The other parameters are m=1, n=10, N=2000, q=1 and k=2.

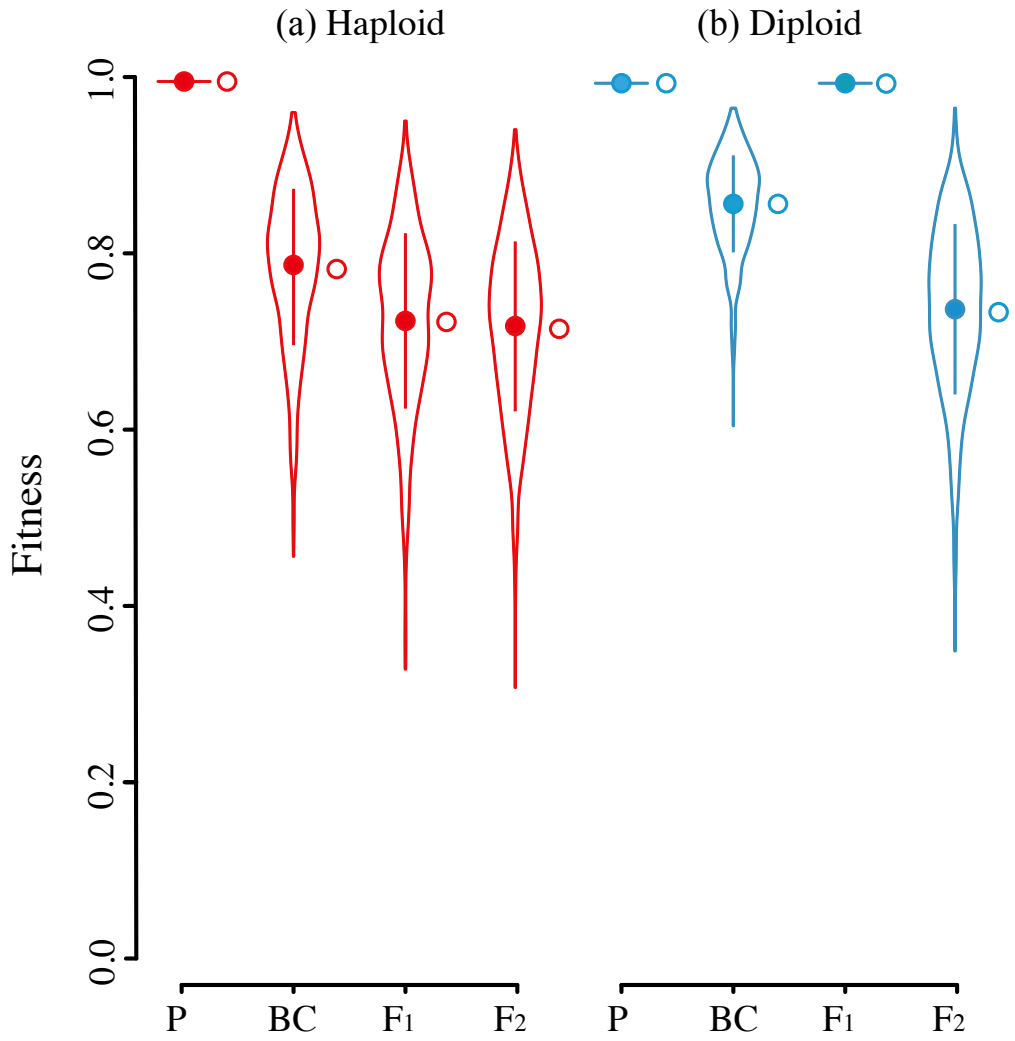

Figure 2. Mutation-order speciation and fitness of hybrids in (a) haploids and (b) diploids. We arbitrarily consider population 1 to be the "local" population used as the backcross parent, BC_L (backcross results using the "foreign" population 2, BC_F, are similar). The phenotypic optimum was displaced from the origin in one direction by 2, after which mutations were allowed to accumulate (see Table S1). The majority of fitness loss accumulates during the first adaptation phase (open circles). Parameters: m=1, n=10, N=2000, $\lambda = 0.04$, q=1.0, k = 2.0, with distributions and solid points representing the mean ± SD calculated from one simulation. 1000 individuals were generated for each hybrid type.

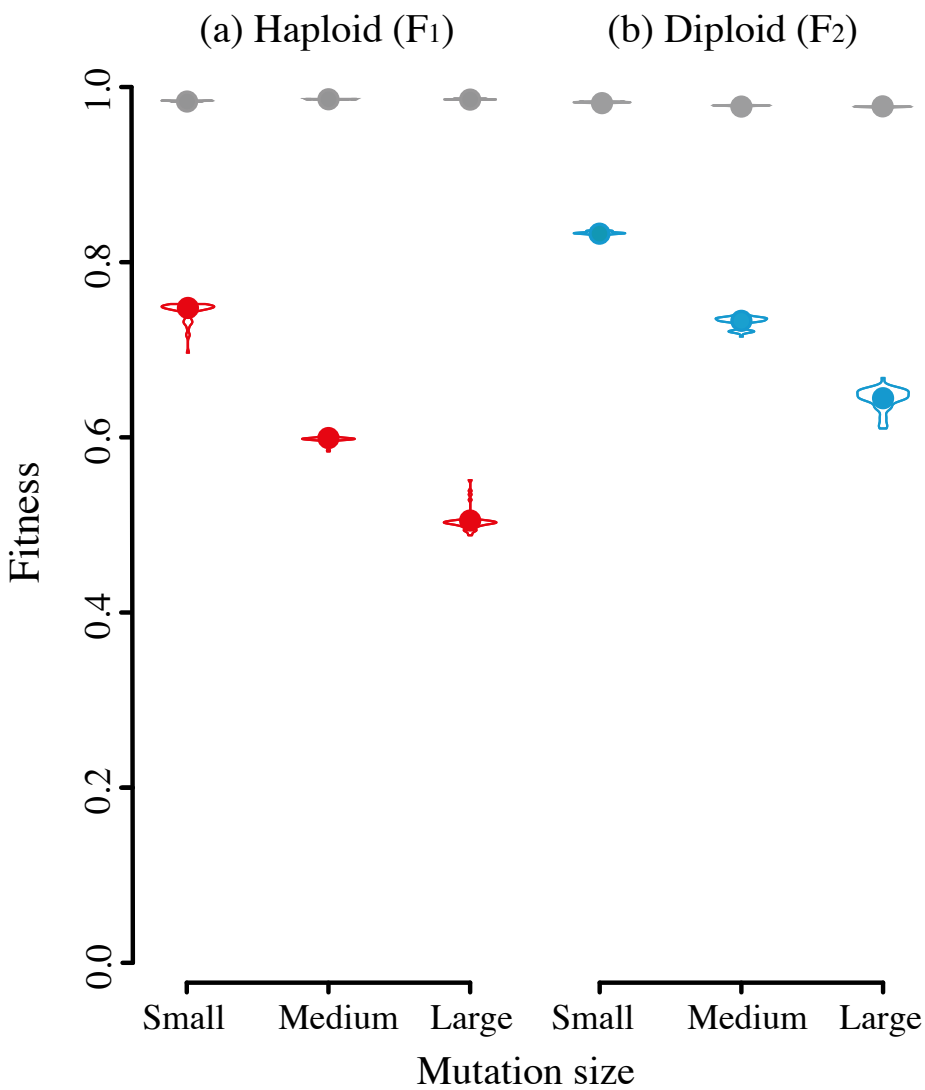

Figures 3. Stronger reproductive isolation arises during mutation-order speciation with large-effect mutations. (a) F_1 hybrid fitness in haploids and (b) F_2 hybrid fitness in diploids when mutations have different average effect sizes. For comparison, grey points indicate the fitness of parental genotypes (arbitrarily using population 1). Mutations are drawn from an exponential distribution with $\lambda = 0.04$ (small), 0.08 (medium), and 0.12 (large). All other parameters are as in Figure 2 except that this figure is calculated from 50 simulations.

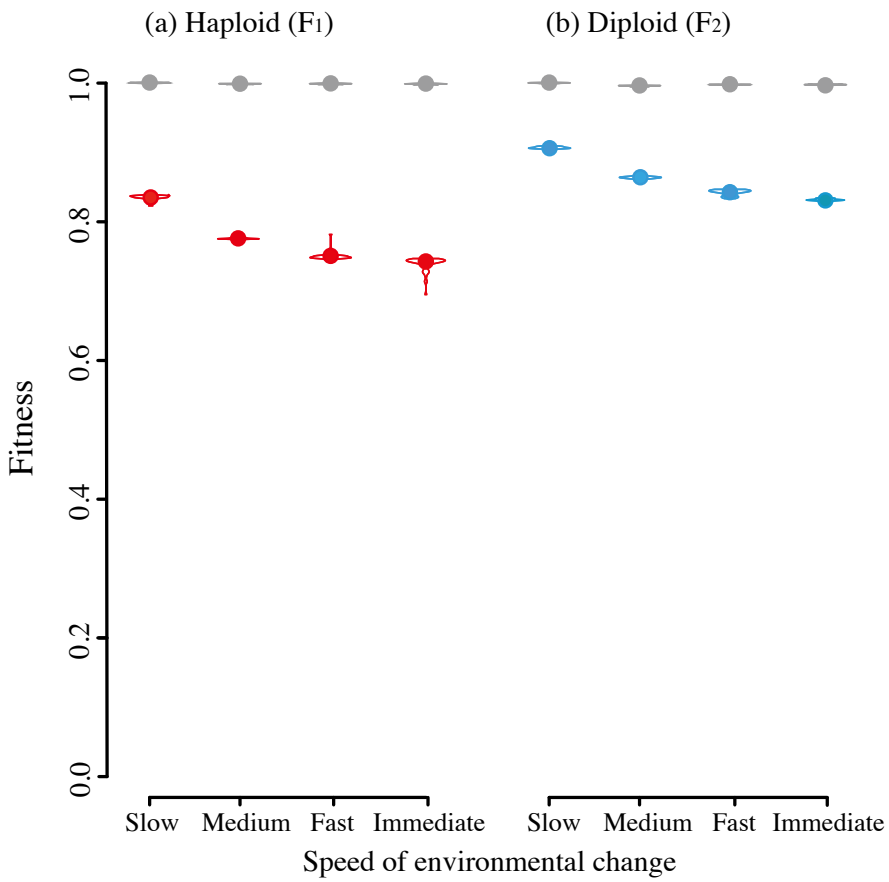

Figure 4. Stronger reproductive isolation arises during mutation-order speciation with a faster changing environment. (a) F_1 hybrid fitness in haploids and (b) F_2 hybrid fitness in diploids when the optimum moves at different speeds. The optimum is gradually moved from the origin in one trait dimension over $\tau = 100$ (slow), 50 (medium), 20 (fast) or 0 (immediate) fixation events until the new optimum is reached. Grey points show the fitness of the parental genotypes. All other parameters are as in Figure 3 with $\lambda = 0.04$; data for $\tau = 0$ are identical to Figure 3 for small-effect mutations.

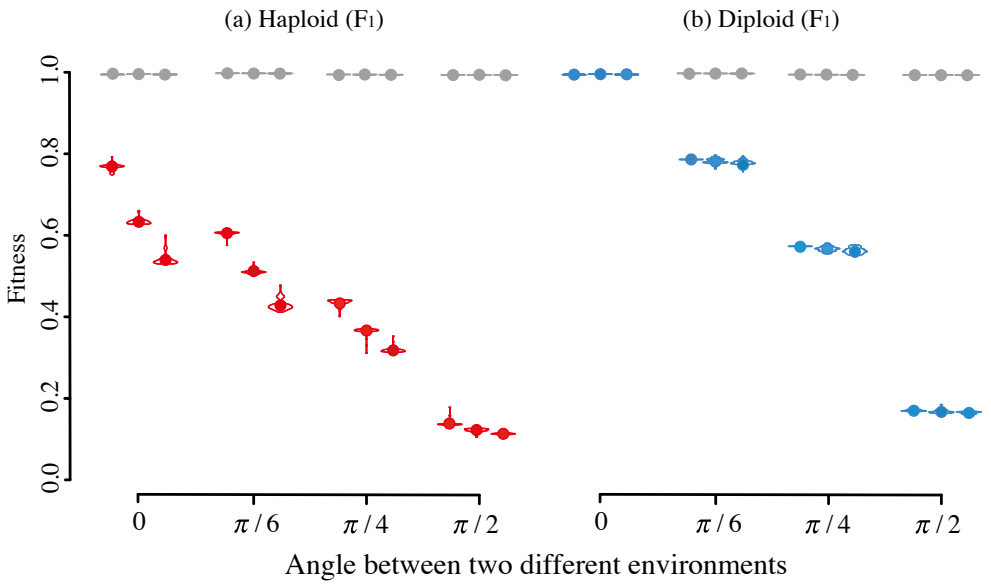

Figure 5. F_1 fitness under ecological speciation as two populations adapt to optima at different angles with respect to the origin and with different average mutation sizes in (a) haploids and (b) diploids. Mutations are drawn from an exponential distribution with $\lambda = 0.04$, 0.08, and 0.12 (three adjacent points from left to right). Grey points show the fitness of the parental genotypes. All other parameters are as in Figure 3.

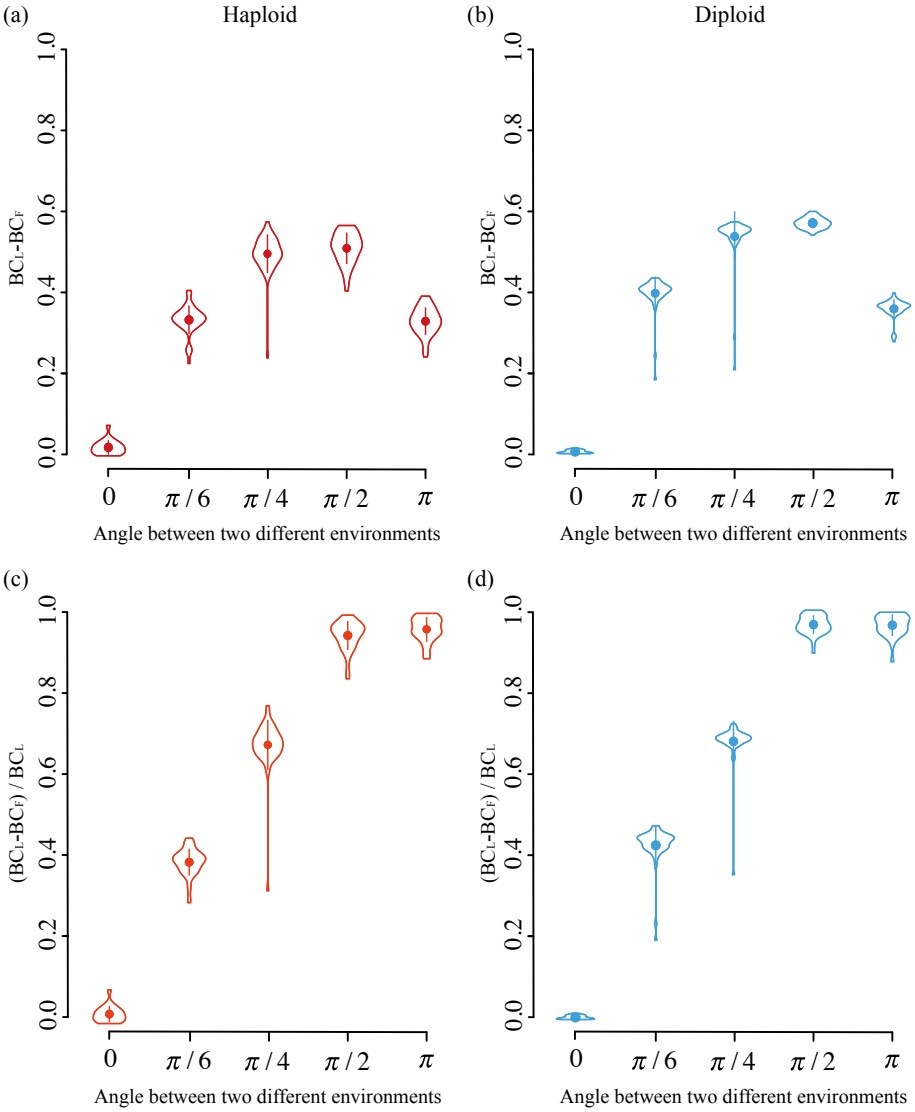

Figure 6. Estimating the degree of ecologically-dependent reproductive isolation. Top panels give $BC_L - BC_F$ for (a) haploids and (b) diploids, as a function of the angle between the optima toward which the parental populations were evolving. Bottom panels give $(BC_L - BC_F)/BC_L$ for (c) haploids and (d) diploids. While $BC_L - BC_F$ shows a non-monotonic relationship, $(BC_L - BC_F)/BC_L$ rises monotonically with the degree of ecological difference between the two environments. Mutations are drawn from an exponential distribution with $\lambda = 0.04$ (small). All other parameters are as in Figure 2, with distributions and solid points representing the mean $\pm$ SE calculated from 50 simulations.

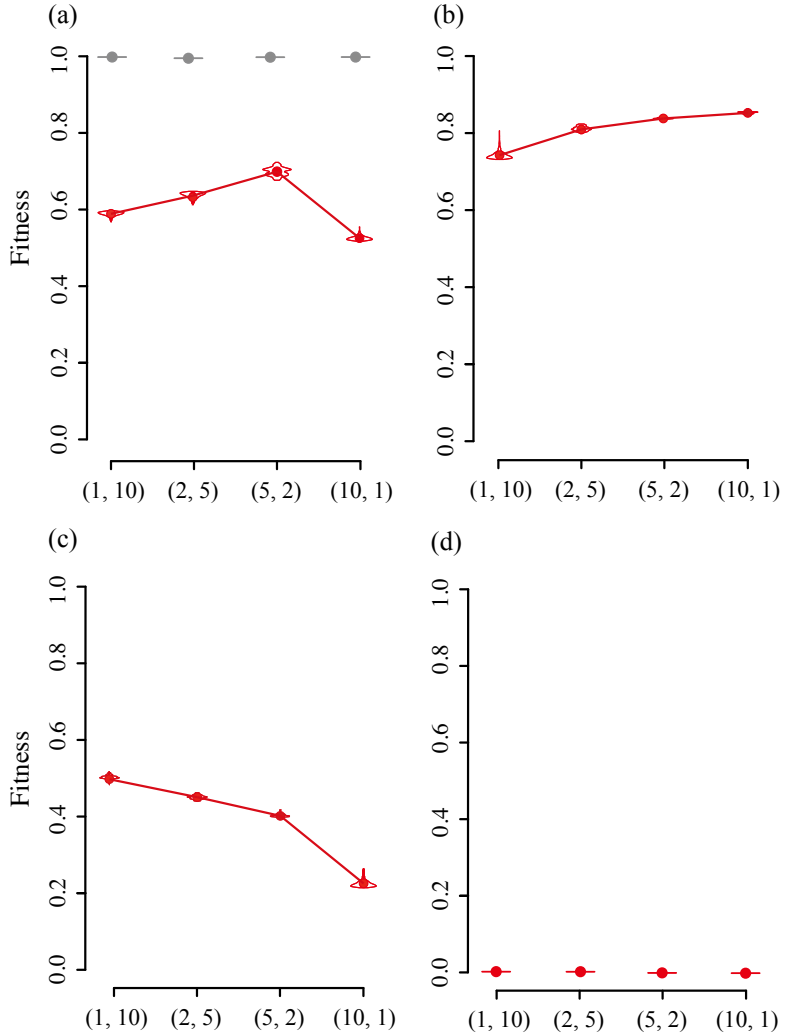

Figure 7. Effect of modularity on the accumulation of reproductive isolation in haploid F_1 hybrids. Panel (a) includes all mutations fixed, while (b) includes only the first 50% of mutations fixed during the adaptation phase and (c) includes only the second 50% of mutations fixed during the adaptation phase; panel (d) includes only mutations fixed during the circling phase. In each case, the phenotypic effects were added to parents whose phenotypes were at the origin. All other parameters are as in Figure 2, except that this figure changes the number of spheres along the x-axis (1 on left and 10 on right) and is calculated from 50 simulations.

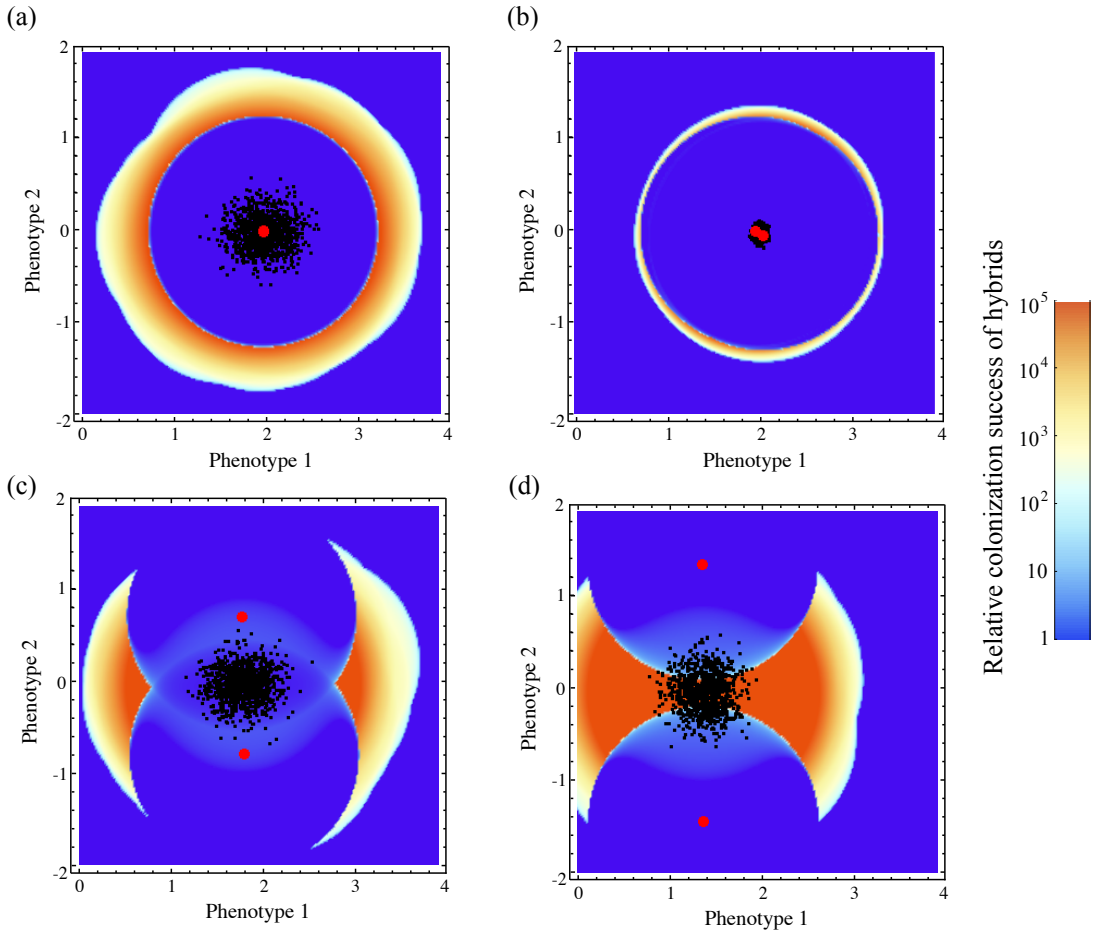

Figure 8. Establishment probability of hybrids relative to parents when colonizing a new environment. Color scale gives the factor by which the mean establishment probability of hybrids is greater than the mean establishment probability for the two parents, ranging from hybrids being 100,000 times more likely to establish (red) to hybrids being less than or equally likely to establish (blue). Fixation probabilities $<10^{-6}$ were set to 10^{-6} to avoid division by small numbers. (a) Mutation-order speciation with an optimum shifted by 2, as in Figure 2. (b) Mutation-order speciation using the subset of mutations in panel (a) that occurred only during the circling phase, assuming that both populations started with the same phenotype, at the optimum, after the adaptation phase. (c) Ecological speciation with an angle between the two optima of $\pi/4$. (d) Ecological speciation with an angle of $\pi/2$, as in Figure S3. Black and red dots represent the phenotypes of hybrids and parents, respectively. All other parameters are as in Figure 2; in addition, $b = 5$.

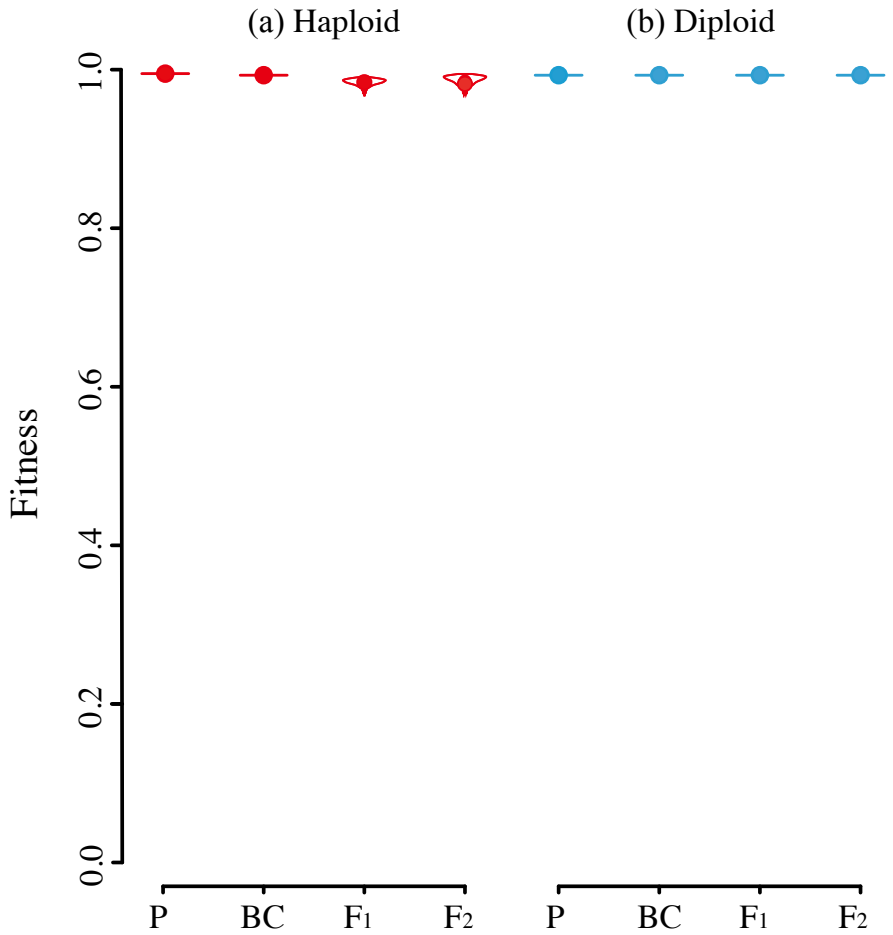

Figure S1. Little reproductive isolation arises during mutation-order speciation during the circling phase in (a) haploids or (b) diploids. See Table S2 for the number of events, as given for Figure 2. All other parameters are as in Figure 2.

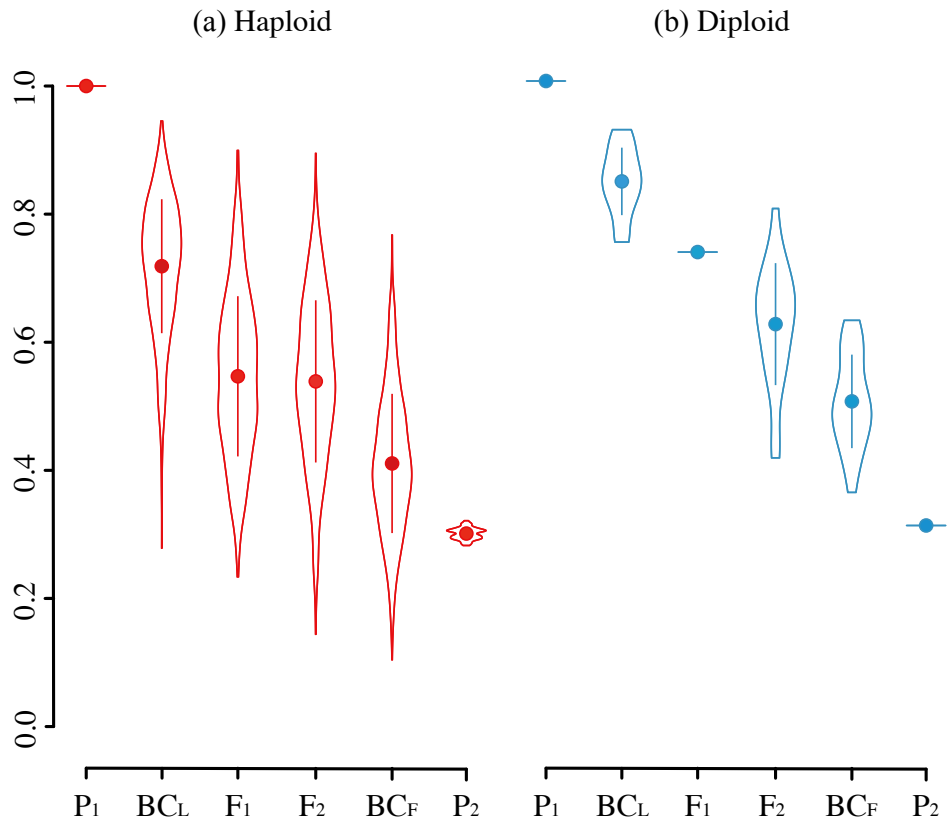

Figure S2. Ecological speciation and the fitness of hybrids in (a) haploids and (b) diploids. Figure is identical to Figure 5 except that the angle between the two optima is $\pi/6$.

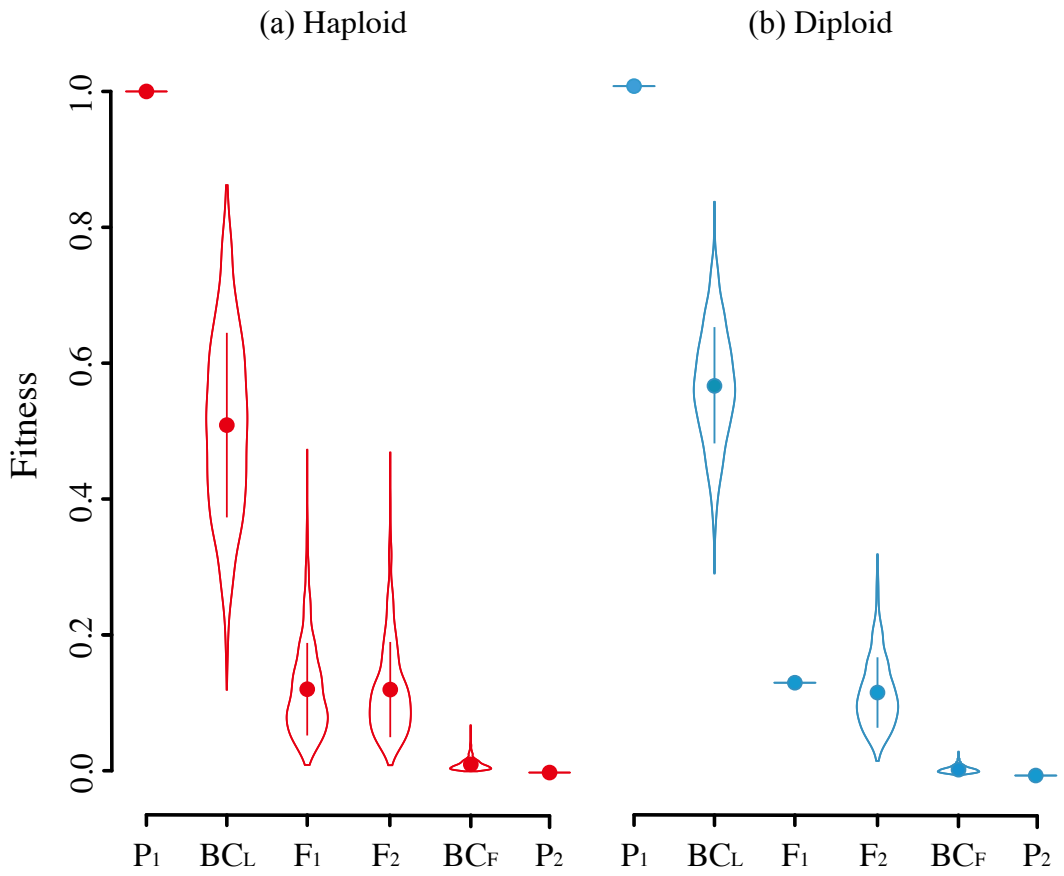

Figure S3. Ecological speciation and fitness of hybrids in (a) haploids and (b) diploids. We illustrate the case where the "local" environment is that of population 1 (P_1). The angle between the optima of the two environments is set to $\pi/2$, relative to the origin (see Table S1 for details). All other parameters are as in Figure 2, with distributions and solid points representing the mean $\pm$ SD calculated from one simulation. 1000 individuals were generated for each hybrid type.